Available online at www.sciencedirect.com

ScienceDirect

Acta Materialia 75 (2014) 147–155

Acta MATERIALIA

www.elsevier.com/locate/actamat

Impact of nanodiffusion on the stacking fault energy in high-strength steels

T. Hickel *, S. Sandlöbes, R.K.W. Marceau [1], A. Dick, I. Bleskov, J. Neugebauer, D. Raabe

Max-Planck-Institut für Eisenforschung GmbH, D-40237 Düsseldorf, Germany

Received 20 September 2013; received in revised form 20 March 2014; accepted 27 April 2014
Available online 2 June 2014

Abstract

A key requirement of modern steels – the combination of high strength and high deformability – can best be achieved by enabling a local adaptation of the microstructure during deformation. A local hardening is most efficiently obtained by a modification of the stacking sequence of atomic layers, resulting in the formation of twins or martensite. Combining ab initio calculations with in situ transmission electron microscopy, we show that the ability of a material to incorporate such stacking faults depends on its overall chemical composition and, importantly, the local composition near the defect, which is controlled by nanodiffusion. Specifically, the role of carbon for the stacking fault energy in high-Mn steels is investigated. Consequences for the long-term mechanical properties and the characterisation of these materials are discussed.

Keywords: Stacking fault energy; Iron; Carbon; In situ TEM; DFT

1. Introduction

In order to combine high strength and high ductility in steels, adaptive microstructures are required, which allow the material to react only locally to potential failure mechanisms caused by high stress levels. This adaptation can occur by diffusionless (martensitic) transformations to another well-defined crystal structure – the so-called transformation induced plasticity (TRIP) mechanism; alternatively, materials showing twinning-induced plasticity (TWIP) make use of twin boundary formation, accommodating strain and creating obstacles for dislocation motion.

Both deformation processes can be realised by locally modifying the sequence of atomic layers in the affected region [1]. However, this is only possible if the energy to create the change in stacking sequence – the stacking fault energy (SFE) – is sufficiently low. Therefore, the SFE serves as an indicator for the occurrence of either of the aforementioned deformation mechanisms. The observation that adjusting the SFE influences the adaptation of the microstructure allows new routes in designing damage-tolerant, high-strength steels with tailored mechanical properties [2].

Changing the chemical composition of a material is the most suitable strategy for such an adjustment. Austenitic steels, for example, in which the face-centred cubic (fcc) crystal structure is stabilized by a high Ni or Mn content (above 20 wt.%) and a C content of the order of 1 wt.% form an important class of adaptive structural materials. It is generally accepted that the SFE in high-Mn steels is of the order of 20 mJ m^{-2} and that a reduction by about 5 mJ m^{-2} changes the dominant deformation mechanism from TWIP to TRIP [1]. However, compiling experimental results for the dependence of the SFE on the C content in steels reveals strikingly inconsistent trends: some sets of

* Corresponding author.
E-mail address: t.hickel@mpie.de (T. Hickel).
[1] Present address: Institute for Frontier Materials, Deakin University, 75 Pigdons Road, Geelong, VIC 3216, Australia.

http://dx.doi.org/10.1016/j.actamat.2014.04.062
1359-6454/

experiments show only a slight change [3], whereas others report a steep increase in the SFE with C content [4] (see Fig. 1(a)). The discrepancies between the various experiments deviate more than an order of magnitude from the desired accuracy of 5 mJ m^{-2}. Consequently, the reliability of determined values of the SFE (Fig. 1) is debated in the literature [3,5].

Here, we demonstrate that knowing the defect-mediated local chemical composition is critical for understanding and interpreting the origin of the conflicting experimental data. This finding goes beyond the above cited studies, which assume a homogeneous atomic compositions of the steel samples. Instead, we bring experimental observations into context with the Suzuki [6] effect. The thermodynamics of segregation of solute atoms to stacking faults was first introduced several decades ago [7,8]. The energetics involved in such a process can be interpreted as the chemical driving force for local diffusion, but also as a way to reduce the SFE as a function of temperature [9]. These concepts are predominantly reported for substitutional elements that are attracted by the stacking fault (SF). In contrast to this, the C atoms behind the discussion in this paper are interstitials that are repelled from the SF. While the absolute changes in the local concentrations might be smaller in such a case, the jumps happen on a different timescale and potential energy surface than vacancy-mediated bulk diffusion. In addition, we were able to prove by ab initio calculations that just a few atomic jumps of interstitial carbon out of the SF are sufficient to substantially lower its energy. In this respect, C probably behaves similarly to, for example, nitrogen in high-N steels, for which an increase in the SFE has also been revealed by ab initio [10]. Based on the insights obtained in this work, we provide experimental evidence for such a Suzuki effect and its relevance for macroscopic deformation in high-Mn steels.

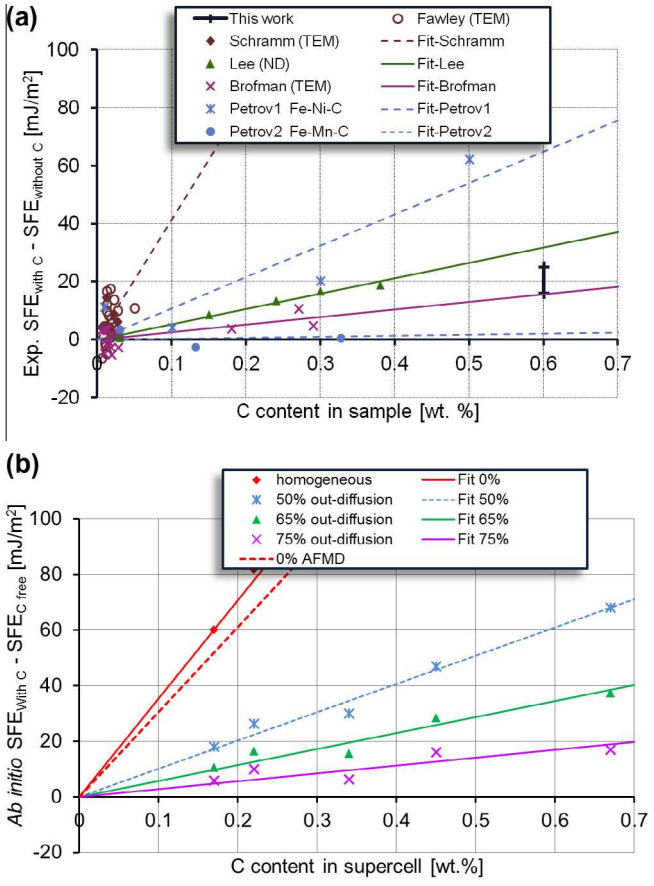

Fig. 1. Dependence of the stacking fault energy (SFE) in Fe–C based austenitic alloys on the C concentration. (a) Experimental data [3,4,11–13] using different techniques (X-ray diffraction, neutron diffraction and transmission electron microscopy) yield conflicting trends for the SFE. Dashed lines indicate less reliable extrapolations due to the sparseness of experimental data. The black bar indicates our experimental result (see Section 5) for the absolute changes for the SFE within the same sample due to nano-diffusion. (b) Ab initio calculations for the SFE in Fe–C assuming different distributions of C atoms. The red symbols correspond to a completely homogeneous C distribution. The impact of the Suzuki effect, where a certain percentage of the C atoms (see legend) diffuses out of the atomic layers that form the stacking fault is shown by blue, green and purple symbols. (For interpretation of the references to colour in this figure legend, the reader is referred to the web version of this article.)

2. Ab initio methodology

To resolve the controversy about the role that C plays for the SFE, we have first used density functional theory (DFT), which allows us to focus on the influence of C without being simultaneously confronted with the full complexity of multicomponent and magnetic steels. The DFT calculations were carried out with the Vienna ab initio simulation package (VASP) [14] using the projector-augmented wave basis set [15] and the PBE exchange–correlation functional. Explicit calculations of intrinsic stacking faults as well as calculations using the axial next-nearest-neighbour Ising (ANNNI) [16] approach have been performed. A numerical convergence of the stacking fault energy values, in the sense that an interaction of ISFs with their periodic images becomes negligible (<1 mJ m^{-2}), was obtained for supercells with a minimum of six atomic layers. The independence of the SFE on the particular set-up is ensured by a comparison with recently published results [17]. For the non-magnetic results in Fig. 1(b), one carbon atom in supercells starting from 32 up to 128 Fe atoms has been used and the independence of the atomic configuration has been ensured [18]. Atomic relaxation of the internal atomic positions perpendicular to the stacking fault have been included. Furthermore, a comparison of the non-magnetic approach (solid lines in Fig. 1(b)), with a complete antiferromagnetic double-layer (AFMD) calculation (red dashed line in Fig. 1(b)), has been performed to ensure the independence of the C trend with respect to magnetism. Other numerical parameters were chosen such that a precision of energies within 10^{-5} eV $atom^{-1}$ (corresponding to errors in the SFE below 10 mJ m^{-2}) was achieved. Specifically, an energy cut-off of 400 eV and a k-point mesh of $8 \times 8 \times 8$ for a $2 \times 2 \times 2$ fcc cell as well as $6 \times 12 \times 7$ for a $4 \times 2 \times 2$ hexagonal close-packed

(hcp) cell (ANNNI approach) have been used in the case of the AFMD calculations. Diffusion barriers and paths have been computed employing climbing-image nudged-elastic band (NEB) calculations [19] with VASP using an 82-atom supercell and similar convergence criteria as in the energy calculations above. The k-point mesh employed in this case was $8 \times 8 \times 3$.

3. Ab initio results and interpretation

Our initial DFT calculations use the assumption that the C atoms are homogeneously distributed and that the presence of the SF does not trigger nanodiffusion of C atoms. The SFE of fcc Fe–C has been computed for different C concentrations [18] and a strong increase with the C content was observed (red line in Fig. 1(b)). The trend is consistent with the experimental assessment of Schramm and Reed [4], which is historically the first paper to report such a strong influence of C, though it was later shown to suffer from large extrapolation errors [3].

Analysis of our results shows a strong driving force for C to diffuse out of the four layers of hcp metal atoms within the SF (square symbols in Fig. 2). The computed solution enthalpy is highest (i.e. the thermodynamic probability for C to occupy this site is lowest) in the centre of the SF, and then decreases by 0.7 eV in the neighbouring (111) layer of octahedral sites. It drops further in the ensuing layer (1.3 eV less than in the centre of the SF), then remains constant in all the subsequent layers (for details see Ref. [18]). We note, however, that the intrinsic diffusion barrier of C in fcc Fe is rather large.

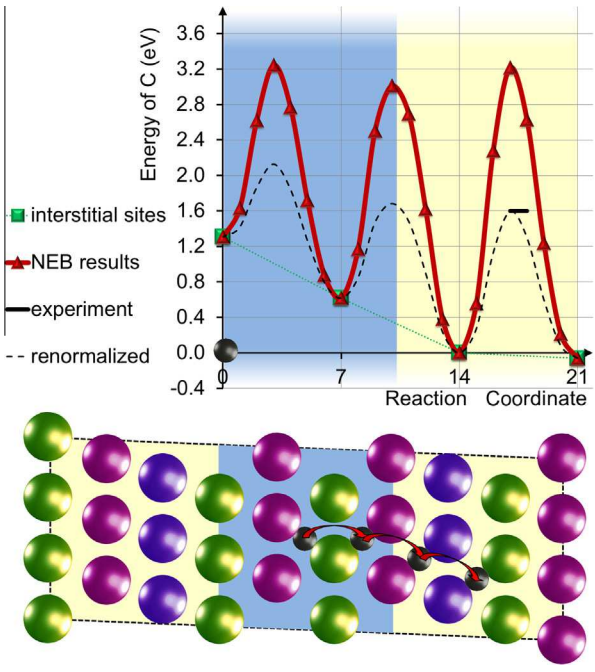

Fig. 2. Non-magnetic ab initio calculation of the energetics of a single C atom along a diffusion path from the centre of the SF into the matrix. The differently shaded areas indicate the hcp (centre of stacking fault) and fcc stacking sequence. The green square symbols (connected by a dotted line as a guide for the eye) provide the C solution enthalpies in the interstitial sites, whereas the red solid line represents the energy barrier for the diffusion. The black dashed line visualises an energy profile obtained after renormalizing the ab initio values to match the experimental value in the bulk fcc region [20,21]. (For interpretation of the references to colour in this figure legend, the reader is referred to the web version of this article.)

The results of an ab initio NEB calculation for the energetics of a single C atom along the minimum energy path from the centre of the SF into the matrix are presented in Fig. 2. The calculation has been performed for a non-magnetic configuration and yields an energy barrier of approx. 3.2 eV in the fcc region next to the SF, which is consistent with previous ab initio calculations [22] for defect-free, non-magnetic fcc Fe. The previous results [22] also demonstrate a strong dependence of the ab initio result on the assumed magnetic state, which motivates a renormalization of the non-magnetic NEB results by a factor 1/2 in order to match the experimental diffusion barriers for C in fcc Fe of approx. 1.6 eV [20,21].

Within the SF, the diffusion barriers are reduced by more than 25%. The reduction of the first barrier (to a renormalized value of less than 1 eV) could be sufficient to allow a jump of C out of the centre layer of the SF when exposed to room temperature for several hours. However, the second barrier within the SF (its renormalized value is ~1.2 eV) kinetically suppresses C diffusion to a large extent. At room temperature, for example, one would have to wait ~40 days for a single jump of a C atom into the fcc region (if the attempt frequency is 10^{13} s^{-1}).

The key question in this work is whether this scenario of suppressed kinetics is also applicable to the experiments that are used to determine the SFE. On the one hand, we argue that this is the case with X-ray (XRD) and neutron (ND) diffraction, where the sample is hardly affected by the experiment. Here, the SFE is indirectly estimated from a relative peak shift of the (111) and (200) reflections when comparing undeformed and slightly deformed samples, which occurs due to the faulting of the fcc crystal structure. An advantage of the method is the statistical average over large bulk volumes. An XRD-based SFE determination was promoted by Schramm and Reed [23,24] for austenitic steels, although it was not used for their data presented in Fig. 1(a). The achievable accuracy with XRD measurements is severely limited by peak broadening and shifting due to inhomogeneous lattice strains. For example, de Campos et al. [25] found a correction by 25% of the values reported in Refs. [4,23,24] without questioning the method itself. More recently, Lee et al. [12,26] have presented a detailed analysis using ND instead of XRD profiles to determine the SFE of tensile-strained bulk samples. Additionally, they sampled a larger range of C compositions [12]. Their data[2] qualitatively confirm the earlier findings

[2] To resolve the dependence on the C concentration, the assessment of the data in the present paper uses a five-component (Cr, Mn, Si, N, C) composition equivalent method instead of the assessment (using C + N, C/N) employed in Ref. [12].

of a strong impact of C, though the effect is less pronounced than in the previous work [4].

Transmission electron microscopy (TEM) experiments, on the other hand, enable direct imaging of stacking faults created by the splitting of a single pair of partial dislocations and are thus considered to give the more reliable data compared to the aforementioned diffraction methods [27]. The calculation of the SFE γ from the splitting d of these partials is based on the relations [27]

$$d_{\text{screw}} = \frac{\mu b^2}{6\pi\gamma}\left(\frac{-1/4}{1-\nu}+3/4\right),$$
$$d_{\text{edge}} = \frac{\mu b^2}{6\pi\gamma}\left(\frac{3/4}{1-\nu}-1/4\right) \quad (1)$$

for screw and edge dislocations with Burger's vector b, respectively. Here, μ is the shear modulus and ν the Poisson's ratio. The assessment of Brofman and Ansell [3], which is solely based on TEM, is also given in Fig. 1(a). Part of their data [11] is identical to that used by Schramm and Reed [4], but additional measurements for samples with a larger C concentration allowed a more reliable conclusion about the dependence of the SFE on the C content. A remarkable finding of these TEM studies is that this dependence is strongly reduced in comparison to the ND results of Lee et al. [12,26]. The effect can be seen even more clearly in the TEM data of Petrov [13] for Fe–Mn–C steels (1(a)).

Our explanation for the discrepancies between the XRD, ND and TEM measurements is the effect of electron irradiation on nanodiffusion of C. Irradiation of solids by an electron beam in TEM measurements induces scattering events that can result in an energy exchange between the electrons and the material. The energy loss due to elastic scattering is approximately given by

$$Q_{\text{el}} = \frac{2\pi n Z^2 r_e^2 mc^2}{\beta^2}\left[\ln\left(\frac{m^2c^4\beta^2}{ZI^2(1-\beta^2)}\right)-\beta^2+0.198\right] \quad (2)$$

and the energy loss due to Coulomb scattering is given by

$$Q_{\text{C}} = \frac{2\pi n Z^2 R^2 mc^2}{1837.5A\beta^2}\ln\left[\frac{E_{\max}}{E_a}\right]. \quad (3)$$

Here, the velocity v of the electrons with mass m in the beam enters via $\beta = v/c$, where c is the speed of light. The energy of the electrons, E, enters via $E_{\max} = 2E(E+2mc^2)/Mc^2$, where M is the relative nucleus mass. Though not thermodynamically correct, the energy exchange is sometimes interpreted as a local temperature increase [28,29] according to

$$\Delta T_e = \frac{3J(Q_{\text{el}}+Q_{\text{C}})}{8cDd}R_e^2\ln\left[1+\frac{4Dt_e}{R_e^2}\right], \quad (4)$$

where t_e is the irradiation time and πR_e^2 is the irradiation area. If one assumes a thermal diffusivity D similar to that in austenitic Fe–Cr–Ni steels and varies the electron beam current density J between 10 and 100 mJ cm^{-2}, the resulting temperature increase in the focus of the electron beam amounts to 175–350 K.

The estimated energy exchange is large and will immediately activate diffusion events that are not possible at ambient temperature. Using representative parameters (250 K for heating and 1.2 eV for the second energy barrier), the rate increases from $\sim 10^{-4}$ to $\sim 10^{4}$ jumps of a C atom per minute. Since the centre of the SF will in any case quickly become free of C (due to the lower barrier in Fig. 2) and only one directional jump is then still needed for the interstitial C atom to leave the hcp region of the SF and to reach the fcc region of the austenitic steel, this is likely to happen during the typical timescale of a TEM experiment. The energy surface for single C atoms in the adjacent fcc region is only slightly affected by the presence of the SF, so the C atoms will be homogeneously distributed in this region.

The outward diffusion (depletion) of C from the SF region leads to a strong decrease in the SFE, very similar to the lowering of dislocation energies by segregation (accumulation) of solute atoms as observed by Suzuki [6]. We note that Suzuki segregation has mainly been attributed to the adsorption of substitutional elements [7–9,30], while the effects observed in this work are favoured by the fact that the motion happens in the opposite direction and involves interstitial atoms. Therefore, one could also label the nanoscale diffusion discussed in the present work as an "anti-Suzuki" effect. In Fig. 1(b) we have used our ab initio data to provide different scenarios corresponding to different fractions of C atoms to follow the driving force of such a Suzuki effect. These results can explain all of the trends observed by different experimental methods (Fig. 1(a)) and also provide an estimate of the amount of C contained in the SF during the measurement.

4. Experimental methodology

To experimentally verify the proposed effect of the electron beam on nanodiffusion of C, we performed in situ cooling–heating experiments on an Fe–22Mn–0.6C wt.% (Fe–22Mn–3C at.%) sample in the transmission electron microscope. For this purpose, high-purity (electrolytically refined) Fe and Mn and pure graphite were melted in an induction furnace under an argon atmosphere and cast into a rectangular copper mould. To obtain a compositionally homogeneous microstructure, the solidified steel slab was subjected to the following sequence of thermomechanical treatment: (i) hot rolling at 1150 °C, with a thickness reduction of 8–10% per pass and a total thickness reduction of 70%; (ii) annealing at 1150 °C under an argon atmosphere for 6 h, followed by water quenching; (iii) hot rolling at 1150 °C, with a thickness reduction of 8–10% thickness reduction per pass to a total thickness reduction of 60%; and (iv) final annealing at 1150 °C for 24 h, followed by water quenching.

The C distribution within this steel was investigated by atom probe tomography (APT) measurements. For this

purpose, needle-shaped specimens were taken from the gauge length of a tensile-deformed sample interrupted at a true strain of $\varepsilon = 0.3$. The needles were prepared by a site-specific in situ lift out technique using an FEI Helios NanoLab 600TM dual-beam focused ion beam/scanning electron mocroscopy (SEM) instrument. APT was conducted using a LEAP 3000X HR instrument (Cameca) operating in voltage mode under an ultrahigh vacuum, with a pulse fraction of 20%, a pulse repetition rate of 200 kHz, a detection rate of 0.005 atoms per pulse and a set-point temperature of 60 K. Tomographic reconstruction was performed with the IVAS 3.6.0 software using the shank angle and tip radius measured by SEM after site-specific preparation.

For the TEM investigations, discs with a diameter of 3 mm and a thickness of 1 mm were cut via spark erosion. The discs were compressed slightly beyond the yield point (0.25–0.5% engineering strain) in a Zwick/Roell Z100 universal testing machine in order to form a small population of isolated dislocations and annealed shortly afterwards at 1150 °C, followed by a final water quench. The discs were then mechanically ground to a thickness of 80–90 μm and electropolished until perforation (Struers Tenupol-5) using an electrolyte solution of 30% nitric acid in methanol.

TEM observations were performed in a Philips CM20 with a LaB_6 filament operated at an acceleration voltage of 200 kV. The samples were cooled down to −150 to −160 °C in a GATAN anti-contamination holder filled with liquid nitrogen. One should note that a temperature-dependent experiment has also been proposed by Remy [9,31] and by Gallagher [32] for several fcc alloys (Ag, Cu, Ni and Fe–Mn–Cr-based alloys). Considering the ab initio analysis of the importance of C nanodiffusion in the current work, in retrospect it was a shortcoming of their procedure to start with TEM measurements at room temperature and not in a cooled state. Under these conditions, as pointed out above, most of the C atoms will leave the SF at the beginning of the TEM experiment and nanodiffusion will be absent in subsequent cooling–heating cycles. Therefore, a critical component in our approach was to carefully control the TEM measurement so that the electron beam starts only when the cooling is completed. After observations under cooled conditions, the samples were heated in situ to +40 °C and again cooled to −150 to −160 °C. This procedure was conducted to reveal the effect of sample heating induced by the electron beam on the outward diffusion of carbon (as measured by the change in SF width) during the period of observation.

5. Experimental results and discussion

A prerequisite for discussing the outcome of the in situ cooling–heating TEM measurements is the knowledge of the C distribution in the steel samples. A typical set of APT data is shown in Fig. 3. The left tomogram shows the distribution of C atoms, whereas the right shows an isodensity surface at 1.5 C atoms nm^{-3}. Two one-dimensional concentration profiles have been provided, corresponding to sections within the cylindrical regions of interest as shown, each having a 10 nm diameter and a 100 nm length. These concentration profiles were created using bin widths of 0.5 nm, containing 35 carbon atoms on average (~1150 atoms per bin). They have been taken from areas of high and low density of carbon (relative to

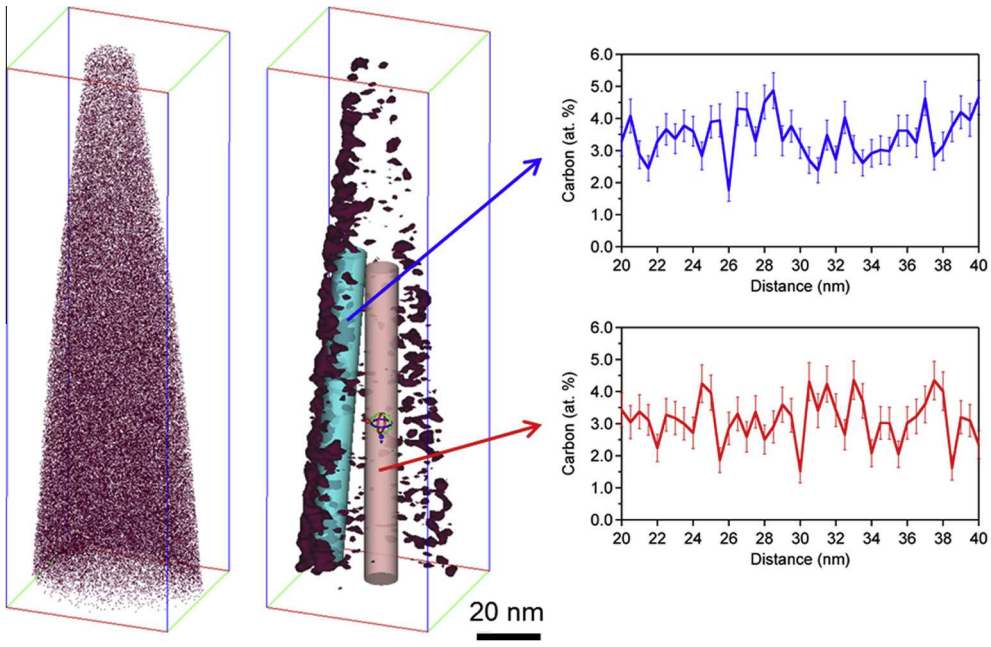

Fig. 3. APT study of the bulk austenitic phase. The tomogram on the left shows the distribution of C atoms and the one on the right shows an isodensity surface at 1.5 C atoms nm^{-3}. The cylinders indicate the regions of interest from which one-dimensional concentration profiles were calculated (see details in text). The measurements indicate relative fluctuations of the local carbon concentration of up to 25%.

the position of the isodensity surface, as indicated), demonstrating the effect of the crystallography of the specimen on the field evaporation of carbon [33]. The measurements indicate that the C distribution is not perfectly homogeneous, but that relative fluctuations of the local carbon concentration of up to 25% can occur on a scale of a few nanometres. These fluctuations alone, however, are insufficient to explain the observed deviations in the experimental SFEs.

By performing the TEM measurements on a cooled sample, the mobility of carbon is suppressed in comparison to experiments made at room temperature. The cooling will reduce, but not eliminate, the impact of scattering events due to the electron beam. During the time that the region of interest, i.e. the partial dislocations that form an SF, was in the direct focus of the electron beam (approx. 10 min.), each C atom in the SF has made one atomic jump on average. Since it is technically too challenging to follow the change of the SF on this timescale, the sample was instead heated in situ to 40 °C, while maintaining the sample position and orientation. It was found in all in situ heating experiments that the dissociation width of the partial dislocations increased by about 40–60% (see e.g. Fig. 4 and Table 1). This corresponds to a decrease in the SFE by ~1/3 of its original value. The magnitude of this change (~9 mJ m^{-2}) is indicated by the black bar in Fig. 1. The observation is in excellent agreement with the difference between the ND measurements of Lee et al. [12,26] and the TEM measurements used by Brofman and Ansell [3], and supports the theoretical interpretation of local diffusion of C out of the SF and into the adjacent fcc phase during the TEM investigation.

There are a number of reasons other than the proposed Suzuki effect that could be given to explain the current TEM observations:

1. A temperature dependence of the free energies of the involved crystal phases (fcc, hcp) that enter the mathematical expression for the SFE.
2. A thermally induced change in the magnetic and/or chemical order.
3. A thermally induced change in local stresses and elastic constants.
4. A thermally activated unpinning of partial dislocations, as well as the reduction of the internal stress level by neighbouring dislocations, free surfaces, etc.

An important indicator that can be used to check the relevance of these mechanisms is the reversibility of the change in dissociation width of the partial dislocations in heating–cooling cycles. The first three items listed above cause reversible changes of the SF dissociation width with temperature. Our interpretation of a Suzuki effect, on the other hand, corresponds to a directional diffusion of C following the driving force to leave the hcp region of the SF, which is an irreversible process.

The reversibility of the temperature effect was tested during the TEM experiments by performing an additional in situ cooling of the sample, directly after heating. For

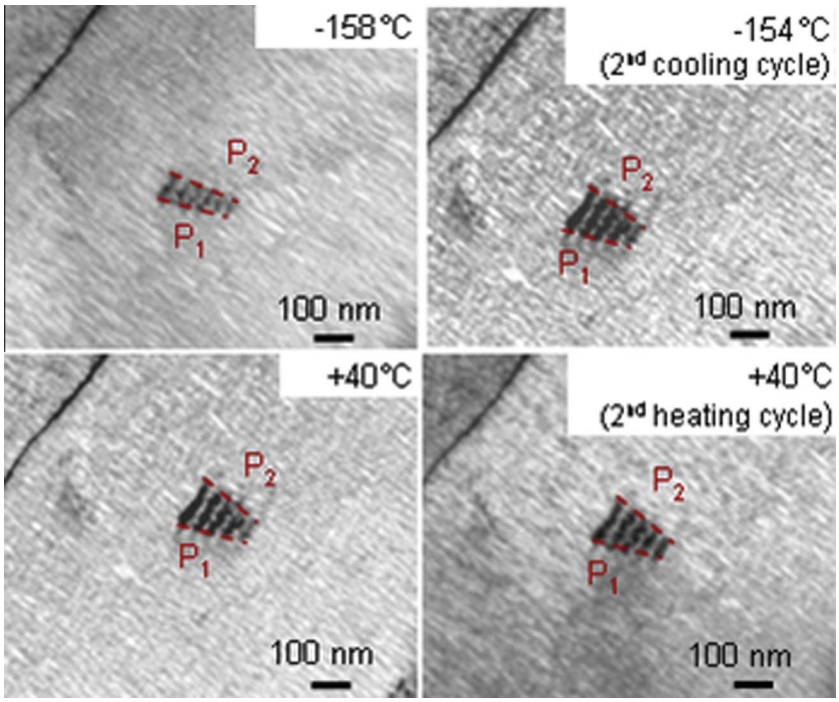

Fig. 4. Change in the dissociation width in Fe–22Mn–0.6C (wt.%) during in situ cooling and heating in the transmission electron microscope. The oscillation contrast of the SF of the pre-deformed sample (0.5% engineering strain) has been obtained under adjusted diffraction conditions. During the first cooling–heating cycle (left-side micrographs), the dissociation width of the partial dislocations has increased. A further cooling–heating cycle (right-side micrographs) did not cause significant changes in the SF width (see also Table 1).

Table 1
Dissociation widths of the partial dislocations shown in Figs. 4 and 5. The larger dissociation width for the samples without cooling (+40 °C) corresponds to a smaller SFE value than for the samples with cooling (−158 °C/−150 °C).

Sample	Dissociation width			Decrease of SFE (%)
	With cooling (nm)	Without cooling (nm)	Increase (%)	
Fig. 4 P1/P2	62 ± 2	97 ± 5	56	36
Fig. 5(a) P3/P4	21 ± 2.5	38 ± 4.5	81	45
Fig. 5(a) P1/P2	41 ± 3	58 ± 5.5	41	29
Fig. 5(b)	12 ± 1.5	18 ± 2	50	33

reversibility, a return of the increased dissociation width to the original value would be necessary. However, this was not observed during cooling, nor were any significant changes of the SFE obtained during a further heating cycle (see the right-hand side of Fig. 4). These observations indicate that the increase in the dissociation width is not reversible in the applied temperature range, which, in turn, is a strong indication that the observed changes in the SFE are not due to thermodynamic reasons.

Previous investigations provide additional arguments for this conclusion. As explained above, the experiments of Remy [9,31] and Gallagher [32] do not cover the Suzuki effect, since they started with heated samples. The temperature dependence of the SFE that they detected between 100 and 300 K is relatively weak and also reversible. This effect corresponds to a decrease in the SFE with lowered temperature (the opposite of the trend seen in our study). When considering the impact of thermal expansion and magnetic entropy on the phase stability of fcc and hcp, we can simulate such a decrease with ab initio calculations in the absence of C.

The effect is furthermore consistent with Calphad assessments [34]. The onset of magnetic order [35] as a relevant process can also be ruled out by the argument of reversibility.

The unpinning mechanism mentioned as point 4 in the list is the only alternative to the Suzuki effect, as it could also yield an irreversible temperature dependence. However, it is anticipated that such a purely thermally activated unpinning or breaking away of dislocations is extremely unlikely to occur in the temperature range (about room temperature) used in this study [36]. We can rule out such an explanation because, for all of the partial dislocations investigated, we consistently observed the same increase in the dissociation width of the bounding partial dislocations of about 40–60% when heating from −150 °C to +40 °C (Table 1). In Fig. 5 we provide further evidence in terms of TEM images of the observed SF before and after in situ heating. Note that all specimens were slightly pre-deformed above the yield point (0.25–0.5% engineering strain) prior to TEM observation, to ensure that the SFs were deformation-induced and not grown, for which the

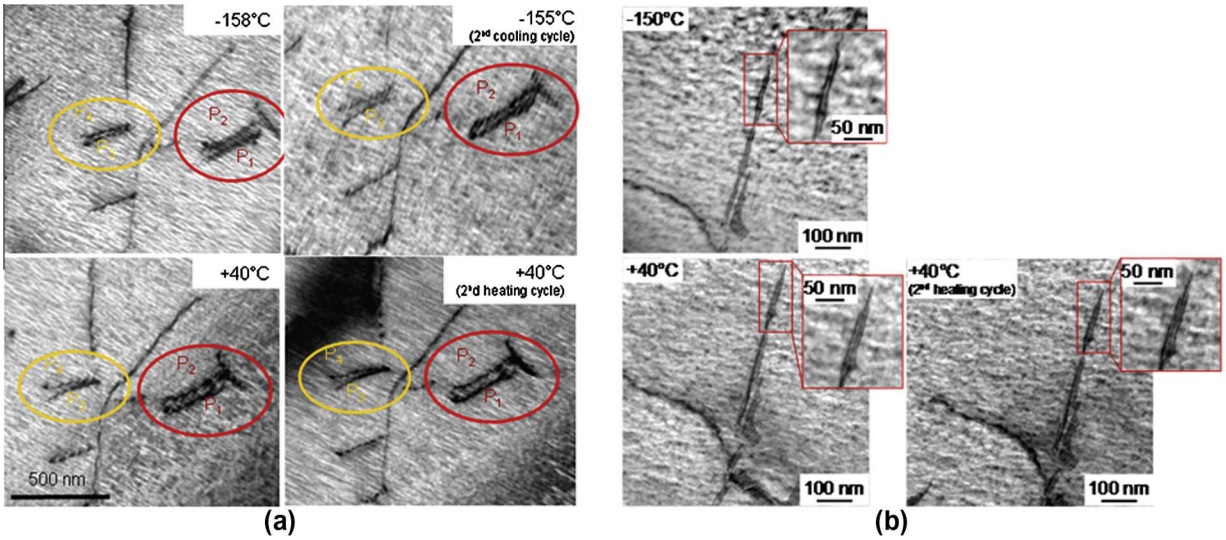

Fig. 5. TEM images of stacking faults with different dissociation widths in Fe–22Mn–0.6C (wt.%) investigated during in situ cooling and heating. The dissociation width of the partial dislocations of the SF increases during the first cooling–heating cycle (see Table 1). No significant changes in the dissociation width are observed during a further heating–cooling cycle (right micrographs). The small dissociation width of the bounding partial dislocations in (b) is due to a small pre-deformation (of only 0.25% engineering strain), while the larger dissociation widths of the samples presented in Fig. 4 and (a) are pre-deformed to a slightly larger degree (0.5 and 0.35% engineering strain, respectively).

C distribution is determined by different temperatures and timescales. Consequently, the measured values for the dissociation width of the bounding partials are not equilibrium values. The sample with the smallest predeformation of 0.25% engineering strain is shown in Fig. 5(b).

While an unpinning effect has been excluded, a pinning effect might be relevant. The C atoms diffusing out of the SF will be trapped by the two partial dislocations, which therefore become less mobile. The now trapped C atoms will influence the value of the SFE and will hinder a further separation of the partials. This might be a reason why the value of the SFE from the current TEM measurements with local heating corresponds not to 100% but to 75% of the outward diffusion (obtained from comparison with ab initio theory; see Fig. 1).

6. Summary and conclusions

The surprisingly large impact of nanodiffusion on the determination of the SFE revealed in this study has implications for the strategies employed to develop adaptive structural materials. In order to control the SFE – and therefore the deformation mechanisms – an approach that is often employed is to modify the global chemical composition of the alloy. The relationship between the global concentrations of alloying elements and the SFE is documented in mechanism maps [37]. The present study reveals that local chemical redistributions can be caused by the deformation mechanisms and can largely modify the corresponding defect energetics.

As indicated by the APT measurements, the distribution of C atoms in the bulk austenite phase is rarely perfectly homogeneous in high-Mn steels. Due to the strong increase in the SFE with C concentration, SFs will form exclusively in regions of the lowest local C content. At ambient conditions, occasional events of nanodiffusion within the SF region will further reduce the local C concentration. Due to the lower diffusion barrier (Fig. 2), this will apply in particular to C atoms in the centre of the SF. The comparison of ND measurements with ab initio calculations in Fig. 1 indicates that the C content could even decrease to 35 % of the global concentration. Therefore, the properties (energy, dissociation width, strain field) of SFs in steels will be determined to a large extent by a local chemical environment that can be significantly different from the global chemical composition. Such a phenomenon for substitutional elements is known as Suzuki segregation [7] and is not limited to steels but, rather, is a general phenomenon [30]. Since this is a systematic effect (i.e. occurring in the same way for all steels deformed at the same temperature), it is implicitly taken into account in previous constructions of mechanism maps.

The prediction of deformation mechanisms becomes particularly difficult if the SFE depends on the experiment performed and its specific set-up. The combination of ab initio calculations and experiments performed in this study clearly proves that TEM measurements at room temperature will modify the region of interest (i.e. the C content in the SF) such that it changes the SFE by approx. 30–40%. Such a strong impact of the measurement on the targeted quantity means that strategies to avoid the influence of the measurement on the result must be taken into account. In TEM, for example, this can be achieved by carefully ensuring that the sample temperature before and during experiment is sufficiently low to prevent atomic jumps in the SF (e.g., by using cooled sampled holders). In the future, mechanism maps for materials with adaptive microstructure should be based on experiments that carefully control nanodiffusion.

This applies not only to the SFE in Fe–Mn–C steels but to all materials with adaptive microstructures where interstitial elements influence critical materials parameters. In particular, we would like to point out that nitrogen [10,38] and hydrogen [39] also yield a clear increase in the SFE in steels, indicating that a similar mechanism as outlined in the present paper for carbon will be relevant for these interstitial solute atoms.

Acknowledgements

The paper benefited from fruitful discussions with Bengt Hallstedt and Joachim Mayer. Funding by the collaborative research centre SFB 761 “Stahl-ab initio” of the Deutsche Forschungsgemeinschaft is gratefully acknowledged. R.K.W.M. gratefully acknowledges the support of the Alexander von Humboldt Foundation through the award of a Humboldt Postdoctoral Fellowship.

References

[1] Frommeyer G, Brüx U, Neumann P. Supra-ductile and high-strength manganese-TRIP/TWIP steels for high energy absorption purposes. ISIJ Int 2003;43(3):438–46. http://dx.doi.org/10.2355/isijinternational.43.438.

[2] Yamakov V, Wolf D, Phillpot S, Mukherjee A, Gleiter H. Deformation-mechanism map for nanocrystalline metals by molecular-dynamics simulation. Nat Mater 2004;3(1):43–7. http://dx.doi.org/10.1038/nmat1035.

[3] Brofman PJ, Ansell GS. Effect of carbon on stacking-fault energy of austenitic stainless-steel. Metall Trans A 1978;9(6):879–80. http://dx.doi.org/10.1007/BF02649799.

[4] Schramm R, Reed R. Stacking-fault energies of 7 commercial austenitic stainless-steels. Metall Trans A 1975;6(7):1345–51. http://dx.doi.org/10.1007/BF02641927.

[5] Rhodes CG, Thompson AW. The composition dependence of stacking fault energy in austenitic stainless steels. Metall Mater Trans A 1977;8(12):1901–6.

[6] Suzuki H. Segregation of solute atoms to stacking faults. J Phys Soc Jpn 1962;17(2):322. http://dx.doi.org/10.1143/JPSJ.17.322.

[7] Ericsson T. On Suzuki effect and spinodal decompostion. Acta Metall 1966;14(9):1073. http://dx.doi.org/10.1016/0001-6160(66)90195-7.

[8] Hirth J. Thermodynamics of stacking faults. Metall Trans 1970;1(9):2367.

[9] Remy L, Pineau A, Thomas B. Temperature dependence of stacking fault energy in close-packed metals and alloys. Mater Sci Eng 1978;36(1):47–63. http://dx.doi.org/10.1016/0025-5416(78)90194-5.

[10] Kibey S, Liu JB, Curtis MJ, Johnson DD, Sehitoglu H. Effect of nitrogen on generalized stacking fault energy and stacking fault widths in high nitrogen steels. Acta Mater 2006;54(11):2991–3001. http://dx.doi.org/10.1016/j.actamat.2006.02.048.
[11] Fawley R, Quader M, Dodd R. Compositional effects on deformation modes annealing twin frequencies and stacking fault energies of austenitic stainless steels. Trans Metall Soc AIME 1968;242(5):771.
[12] Lee TH, Ha HY, Hwang B, Kim SJ, Shin E. Effect of carbon fraction on stacking fault energy of austenitic stainless steels. Metall Mater Trans A 2012;43A(12):4455–9. http://dx.doi.org/10.1007/s11661-012-1423-y.
[13] Petrov Y. Effect of carbon and nitrogen on the stacking fault energy of high-alloyed iron-based austenite. Z Metallk 2003;94(9):1012–6.
[14] Kresse G, Hafner J. Ab initio molecuar-dynamics for liquid-metals. Phys Rev B 1993;47(1):558–61. http://dx.doi.org/10.1103/PhysRevB.47.558.
[15] Kresse G, Joubert D. From ultrasoft pseudopotentials to the projector augmented-wave method. Phys Rev B 1999;59(3):1758–75. http://dx.doi.org/10.1103/PhysRevB.59.1758.
[16] Denteneer PJH, van Haeringen W. Stacking-fault energies in semiconductors from first-principles calculations. J Phys C Solid State Phys 1987;20:L883–7. http://dx.doi.org/10.1088/0022-3719/20/32/001.
[17] Gholizahed J, Draxl C, Puschnig P. The influence of interstitial carbon on the γ-surface in austenite. Acta Mater 2013;61:341–9.
[18] Abbasi A, Dick A, Hickel T, Neugebauer J. First-principles investigation of the effect of carbon on the stacking fault energy of Fe–C alloys. Acta Mater 2011;59(8):3041–8. http://dx.doi.org/10.1016/j.actamat.2011.01.044.
[19] Henkelman G, Uberuaga B, Jonsson H. A climbing image nudged elastic band method for finding saddle points and minimum energy paths. J Chem Phys 2000;113(22):9901–4. http://dx.doi.org/10.1063/1.1329672.
[20] Wells C, Batz W, Mehl R. Diffusion coefficient of carbon in austenite. Trans AIMME 1950;188(3):553–60.
[21] Agren J. A revised expression for the diffusivity of carbon in Fe–C austenite. Scr Metall 1986;20(11):1507–10. http://dx.doi.org/10.1016/0036-9748(86)90384-4.
[22] Jiang D, Carter E. Carbon dissolution and diffusion in ferrite and austenite from first principles. Phys Rev B 2003;67(21):214103. http://dx.doi.org/10.1103/PhysRevB.67.214103.
[23] Reed R, Schramm R. Relationship between stacking-fault energy and X-ray measurements of stacking-fault probability and microstrain. J Appl Phys 1974;45(11):4705–11. http://dx.doi.org/10.1063/1.1663122.
[24] Schramm R, Reed R. Stacking-fault energies of fcc Fe–Ni alloys by X-ray-diffraction line-profile analysis. Metall Trans A 1976;7(3):359–63. http://dx.doi.org/10.1007/BF02642831.
[25] de Campos MF, Loureiro SA, Rodrigues D, da Silva MCA, de Lima NB. Estimative of the stacking fault energy for a FeNi(50/50) alloy and a 316L stainless steel. In: Salgado L, Filho FA, editors. Advanced powder technology VI. Materials science forum, vols. 591–593. Inst Pesquisas Energet Nucl; Metallum Eventos Tecn Cientif; Zürich, Switzerland: Trans. Tech. Pub. Ltd.; 2008. p. 3–7 [Sixth international latin American conference on power technology, Assoc Brasileira Ceram, Buzios, Brazil; Nov. 07–10, 2007].
[26] Lee TH, Shin E, Oh CS, Ha HY, Kim SJ. Correlation between stacking fault energy and deformation microstructure in high-interstitial-alloyed austenitic steels. Acta Mater 2010;58(8):3173–86. http://dx.doi.org/10.1016/j.actamat.2010.01.056.
[27] Hirth J, Lothe J. Theory of dislocations. Wiley; 1982.
[28] Liu L, Risbud S. Real-time hot-stage high-voltage transmission electron-microscopy precipitation of CDS nanocrystals in glasses – experiment and theoretical analysis. J Appl Phys 1994;76(8):4576–80. http://dx.doi.org/10.1063/1.357291.
[29] Yokota T, Murayama M, Howe J. In situ transmission-electron-microscopy investigation of melting in submicron Al–Si alloy particles under electron-beam irradiation. Phys Rev Lett 2003;91(26). http://dx.doi.org/10.1103/PhysRevLett.91.265504.
[30] Finkenstadt D, Johnson DD. Solute/defect-mediated pathway for rapid nanoprecipitation in solid solutions: γ surface analysis in fcc Al–Ag. Phys Rev B 2006;73:024101. http://dx.doi.org/10.1103/PhysRevB.73.024101.
[31] Remy L. Temperature-variation of intrinsic stacking-fault energy of a high manganese austenitic steel. Acta Metal 1977;25(2):173–9. http://dx.doi.org/10.1016/0001-6160(77)90120-1.
[32] Gallagher P. Influence of alloying, temperature, and related effects on stacking fault energy. Metal Trans 1970;1(9):2429.
[33] Marceau RKW, Choi P, Raabe D. Understanding the detection of carbon in austenitic high-Mn steel using atom probe tomography. Ultramicroscopy 2013;132:239–47. http://dx.doi.org/10.1016/j.ultramic.2013.01.010.
[34] Allain S, Chateau JP, Bouaziz O, Migot S, Guelton N. Correlations between the calculated stacking fault energy and the plasticity mechanisms in Fe–Mn–C alloys. Mater Sci Eng A 2004;387–389:158–62.
[35] Gebhardt T, Music D, Ekholm M, Abrikosov IA, Vitos L, Dick A, et al. The influence of additions of Al and Si on the lattice stability of fcc and hcp Fe–Mn random alloys. J Phys Condens Matter 2011;23(24). http://dx.doi.org/10.1088/0953-8984/23/24/246003.
[36] Gavriljuk VG, Shivanyuk V, Shanina B. Change in the electron structure caused by c, n and h atoms in iron and its effect on their interaction with dislocations. Acta Mater 2005;53:5017–24. http://dx.doi.org/10.1016/j.ultramic.2013.01.010.
[37] Saeed-Akbari A, Imlau J, Prahl U, Bleck W. Derivation and variation in composition-dependent stacking fault energy maps based on subregular solution model in high-manganese steels. Metall Mater Trans A 2009;40A(13):3076–90. http://dx.doi.org/10.1007/s11661-009-0050-8.
[38] Mosecker L, Saeed-Akbari A. Nitrogen in chromium-manganese stainless steels: a review on the evaluation of stacking fault energy by computational thermodynamics. Sci Technol Adv Mater 2013;14(3). http://dx.doi.org/10.1088/1468-6996/14/3/033001.
[39] Chakrabarty A, Hickel T, Spatschek R, Neugebauer J; in preparation.